A STABLE ACOUSTIC IMPEDANCE MODEL OF THE CLARINET USING DIGITAL WAVEGUIDES

Gary P. Scavone
CAML, Music Technology Area
Schulich School of Music
McGill University, Montreal, QC, Canada
gary@music.mcgill.ca

Julius O. Smith
CCRMA
Department of Music
Stanford University, Stanford, CA, USA
jos@ccrma.stanford.edu

ABSTRACT

Digital waveguide (DW) modeling techniques are typically associated with a traveling-wave decomposition of wave variables and a "reflection function" approach to simulating acoustic systems. As well, it is often assumed that inputs and outputs to/from these systems must be formulated in terms of traveling-wave variables. In this paper, we provide a tutorial review of DW modeling of acoustic structures to show that they can easily accommodate physical input and output variables. Under certain constraints, these formulations reduce to simple "Schroeder reverb-like" computational structures. We also present a stable single-reed filter model that allows an explicit solution at the reed / air column junction. A clarinet-like system is created by combining the reed filter with a DW impedance model of a cylindrical air column.

1. REFLECTION FUNCTION CALCULATIONS

The use of digital waveguides (DW) to model wave propagation within cylindrical air columns has been well documented [1, 2]. A DW structure like that diagrammed in Fig. 1 can be used to compute the time-domain pressure *reflection function*, $r_p(t)$, of a uniform pipe. The reflection function is defined as the pressure response at the input of an air column caused by the introduction there of a pressure impulse, assuming no reflections at the input end (an anechoic input termination). The digital filter $\mathcal{R}_L$ models the frequency-dependent *reflectance* of the load impedance connected to the far end of the pipe. It can be expressed as

$$\mathcal{R}_L(f) = \left[\frac{Z_L(f) - Z_c}{Z_L(f) + Z_c}\right], \tag{1}$$

where Z_c is the real characteristic wave impedance of the pipe, $Z_L(f)$ is the frequency-dependent load impedance, and f is frequency in Hertz. A closed end is reasonably modeled by a load impedance $Z_L = \infty$, in which case $R_L = 1$. This indicates that pressure traveling-waves reflect from a rigid boundary in a cylindrical pipe with unity gain and no phase shift. For an open end condition, an analytic solution for $\mathcal{R}_L(f)$ has been reported by [3]. A second-order digital filter is sufficient to achieve a good fit to that analytic result for most pipe dimensions of musical interest [4].

The structure of Fig. 1 is a time-domain computational model of one-dimensional traveling-wave propagation along the length of the air column, together with wave reflection from the load impedance at the far end. The frequency-domain counterpart to

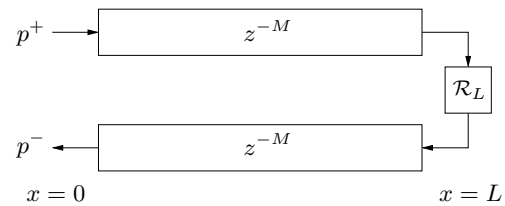

Figure 1: *Digital waveguide model of a cylindrical air column.*

the cylindrical air column reflection function is the plane-wave *reflectance*, which for lossless wave propagation can be written as

$$\mathcal{R}_p(f) = e^{-2jkL}\mathcal{R}_L(f), \tag{2}$$

where the load impedance is located a distance L from the pipe input. Neglecting losses along the air column walls, the phase term in Eq. (2) represents a time delay of $2L/c$ seconds in $r_p(t)$, so that the reflection function is given by a time shifted representation of the reflectance property of the load at the end of the pipe (c is the wave speed of propagation). Within a DW implementation, propagation losses along the air column length can be lumped and commuted with $\mathcal{R}_L$ before the discrete-time filter is designed. As well, the delay-line lengths, M, represented in Fig. 1 can be fractional and implemented with fractional delay techniques [5].

2. IMPULSE RESPONSE CALCULATIONS

The *input impedance* of an air column is defined as its sinusoidal pressure response given the application of a unit sinusoidal volume velocity signal at its input, $Z_0(f) = P_0(f)/U_0(f)$. The input impedance of a cylindrical pipe of length 0.35 meters is plotted in Fig. 2, calculated using a frequency-domain technique [6]. The "peaks and valleys" of this response indicate the resonances

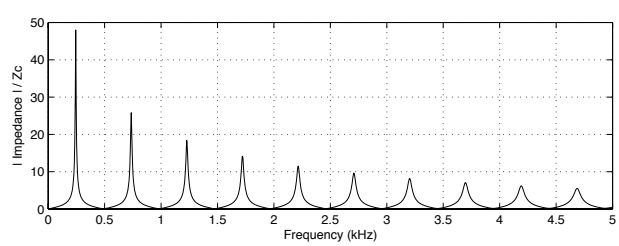

Figure 2: *Theoretical input impedance of a cylindrical pipe of 0.35 meter length.*

and anti-resonances of the acoustic structure, depending on the assumed boundary condition at the input. For example, pressure is ideally constrained to be zero (or equal to the ambient air pressure) at an open end, and thus the resonances of a pipe open at its input end are indicated by the minima of $Z_0(f)$. Likewise, volume velocity is ideally constrained to be zero at a closed end, so that the maxima of the input impedance specify the resonances of a cylindrical structure with a closed input end. The ideal "impedance head" has an infinite "source impedance" [7], which effectively closes the input end.

For a cylindrical pipe terminated by impedance R_L as modeled in Fig. 1, the input impedance can be written in terms of the plane-wave reflectance as

$$Z_0(f) = Z_c \left(\frac{1 + \mathcal{R}_p(f)}{1 - \mathcal{R}_p(f)} \right), \tag{3}$$

indicating that $Z_0(f)$ is completely defined by $\mathcal{R}_p(f)$. Assuming lossless propagation over the length of the air column, $Z_0(f)$ can also be written as

$$Z_0(f) = Z_c \left[\frac{Z_L(f)\cos(kL) + jZ_c \sin(kL)}{jZ_L \sin(kL) + Z_c \cos(kL)} \right], \tag{4}$$

where $k = 2\pi f/c$ is defined as the propagation wave number. This expression can be derived by substitution of Eq. (2) in Eq. (3).

The time-domain description of linear acoustic systems is traditionally given by the inverse Fourier transform of the input impedance, called the *impulse response* $h(t)$ or the Green's function of the system. The impulse response describes the time-domain evolution of pressure at the input of an acoustic structure produced by the injection of a volume velocity unit impulse at the same position. Pressure and flow at the input are then related by means of the convolution product

$$p(t) = \int_0^t h(t - t')u(t')dt' = h(t) * u(t). \tag{5}$$

It is a simple process to extend the DW structure of Fig. 1 to compute the impulse response of an acoustic pipe, as was shown in [4]. The volume velocity impulse at the input is first scaled by Z_c to convert to a corresponding pressure value. The implicit closed-end condition at $x = 0$ is modeled with a reflection coefficient of $+1$ for pressure traveling-wave components. If we are concerned

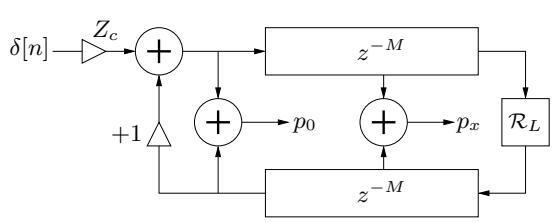

Figure 3: *A digital waveguide cylindrical pipe impedance model (from [4]).*

only with the physical pressure at the input of the acoustic system modeled in Fig. 3, it is possible to commute the two delay lines to form the structure of Fig. 4. The transfer function of the system modeled by Fig. 4 is given by

$$H(z) = Z_c \left(\frac{1 + z^{-2M}\mathcal{R}_L(z)}{1 - z^{-2M}\mathcal{R}_L(z)} \right), \tag{6}$$

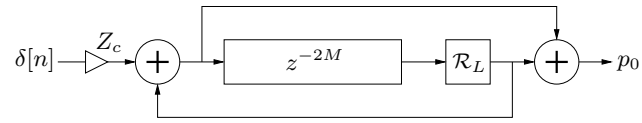

Figure 4: *The commuted digital waveguide input impedance model of a closed-open cylindrical pipe.*

which is equivalent to Eq. (3) with the substitution specified by Eq. (2). The DW structures shown in Figs. 3 and 4 provide efficient computational schemes that support the use of input and output physical acoustic variables, though the structure in Fig. 3 more clearly indicates how to extract physical output variables to be probed at arbitrary positions along the pipe. It is also possible to modify these structures to support the computation of volume flow rather than pressure.

The theoretical input impedance and impulse response of a cylindrical pipe terminated with a load impedance as determined by [3] is shown in Fig. 5, calculated using both a frequency-domain technique [6] and the DW structure of Fig. 4. Propagation losses along the length of the pipe were ignored in both cases.

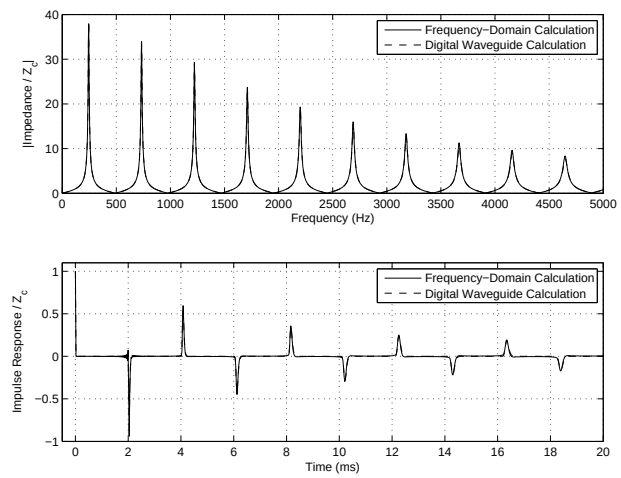

Figure 5: *Calculated input impedance (top) and impulse response (bottom) of a cylindrical pipe of 0.35 meter length.*

A recent paper [8] takes an acoustic modeling approach based on the input impedance transfer function with ideal boundary conditions. That is, by starting with Eq. (4) and assuming an ideal open-end load impedance $Z_L = 0$, $Z_0(f)$ can be written

$$\begin{aligned} Z_0(f) &= Z_c \left[\frac{1 - e^{-2jkL}}{1 + e^{-2jkL}} \right] \\ &= Z_c \left[\frac{1}{1 + e^{-2jkL}} - \frac{e^{-2jkL}}{1 + e^{-2jkL}} \right]. \end{aligned} \tag{7}$$

From the expression of Eq. (7), they propose a computational structure as shown in Fig. 6. As noted by [2, p. 52], this structure can be simplified to the one delay-line form shown in Fig. 7, which is reminiscent of the Schroeder allpass filter used for artificial reverberation [9]. We see that this is equivalent to the structure of Fig. 4, except that the DW approach allows an arbitrary load impedance characterization. In this sense, the DW approach makes it obvious how to achieve the same level

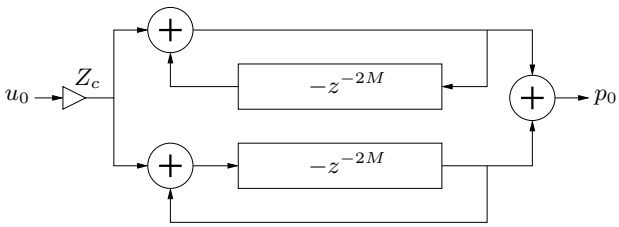

Figure 6: *Ideal impedance transfer function model of cylindrical pipe assuming $Z_L = 0$.*

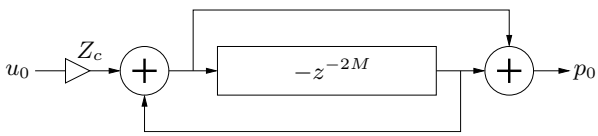

Figure 7: *One-delay form of ideal impedance transfer function model of cylindrical pipe assuming $Z_L = 0$.*

of efficiency while taking into account an acoustically accurate model of open-end reflection and radiation. As previously noted, propagation losses are easily accounted for in the DW structure and typically commuted with the load impedance reflection filter [4].

3. CONICAL IMPEDANCE MODELING

The analyses made for the cylindrical pipe can be repeated for a truncated conical acoustic structure, as diagrammed in Fig. 8. In general, the relationships are a bit more complicated given that the characteristic impedance for spherical waves is dependent on both frequency and position.

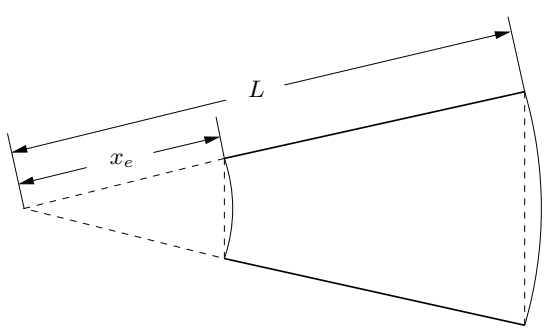

Figure 8: *A conical acoustic structure, truncated at $x = x_e$.*

For a conic section terminated by a load impedance $Z_L(f)$ at $x = L$, the spherical-wave pressure reflectance is given by

$$\mathcal{R}_s(f) = e^{-2jkL}\left[\frac{Z_L(f)Z_c^*(L,f) - Z_c(L,f)Z_c^*(L,f)}{Z_L(f)Z_c(L,f) + Z_c(L,f)Z_c^*(L,f)}\right], \tag{8}$$

where the spherical wave impedance $Z_c(x,f)$ is

$$Z_c(x,f) = \frac{\rho c}{S(x)}\left(\frac{jkx}{1+jkx}\right) = \frac{\rho c}{S(x)}\left(\frac{1}{1+\frac{1}{jkx}}\right), \tag{9}$$

ρ is the mass density of air, c is the speed of wave propagation, and $S(x)$ is the spherical wavefront surface area at position x. Note that if we assume lossless propagation and an ideal open-end load impedance $Z_L = 0$, Eq. (8) reduces to $\mathcal{R}_s(f) = -e^{-2jkL}$, which is equivalent to the reflectance of an ideally terminated cylindrical pipe. Thus, the DW structure of Fig. 1 (with R_L = -1) can be used to simulate spherical wave propagation as well, though traveling-wave and physical output variables at points downstream from the input must be scaled by $1/x$ to account for the spread of pressure over increasing wavefront surface areas. Benade [10] provides an equivalent circuit for the conical waveguide in terms of a uniform transmission line, two acoustic inertances, and a transformer, as shown in Fig. 9. This representation suggests that a conical air

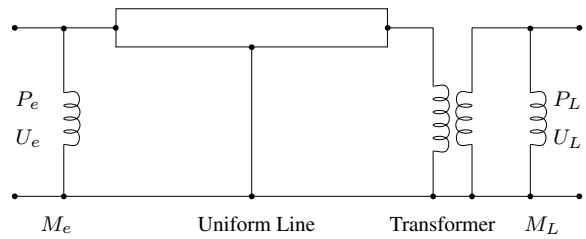

Figure 9: *Equivalent circuit of a conical waveguide.*

column model can be implemented using a cylindrical waveguide, a scalar "turns ratio" multiplier, and appropriately designed inertance components at each end of the waveguide. This interpretation is supported by the expression for the input *admittance* of a conical waveguide,

$$Y_e(f) = \frac{1}{Z_e(f)} = \frac{S(x_e)}{\rho c}\left\{\left[\frac{1-\mathcal{R}_s(f)}{1+\mathcal{R}_s(f)}\right] + \frac{1}{jkx_e}\right\}, \tag{10}$$

where x_e is the length of the missing section of cone at the input. Eq. (10) makes clear the parallel combination of the spherical wave impedance and a term reminiscent of the impedance of a cylindrical waveguide. The inertance term near the output, M_L, can be combined with the output impedance representation and a single digital filter designed. Note, however, that the frequency dependence of this term is inversely proportional to distance from the conic section apex and thus can be ignored in most contexts without having noticeable affect on the resulting response. Further, an ideal load impedance $Z_L = 0$ will "short-circuit" the inertance term and we can expect that a more accurate open-end representation will have similar behavior, especially at low frequencies.

In developing a DW structure to calculate the input impedance of a conic section, the input end, being driven by an ideal velocity source, is terminated by an infinite source impedance, corresponding to a rigid termination. Thus, traveling-wave reflection at this point is completely defined by the input inertance term, M_e, which is represented by a first-order digital allpass reflectance filter of the form [5, 4, 11]

$$\mathcal{R}_e(z) = \frac{-a_1 - z^{-1}}{1 + a_1 z^{-1}}, \quad \text{where} \quad a_1 = \frac{c - \alpha x_e}{c + \alpha x_e}, \tag{11}$$

and α is the bilinear transform constant that controls frequency warping. This first-order allpass filter accounts for the phase delay experienced by pressure traveling-wave components reflecting from a rigid input termination in a conical waveguide.

Impulse response calculations are based on the injection of a volume velocity unit impulse at the input of the system. Because

our DW structure will simulate pressure traveling waves, it is necessary to convert the incoming *flow* impulse to a variable of pressure via the characteristic wave impedance. For cylindrical ducts, Z_c is a real value and simply results in a scaling of the input variable. For conical structures, however, Z_c is a function of frequency and the transformation must make use of a digital filter. Using the bilinear transform, a discrete-time equivalent to Eq. (9) is given by

$$Z_c(x,z) = \frac{\rho c}{S(x)} \left(\frac{\alpha x}{c + \alpha x} \right) \frac{1 - z^{-1}}{1 + a_1 z^{-1}}, \tag{12}$$

where a_1 is equal to the allpass truncation filter coefficient given in Eq. (11). The resulting DW model is represented in Fig. 10. Note that the bilinear transform implicitly performs a continuous-

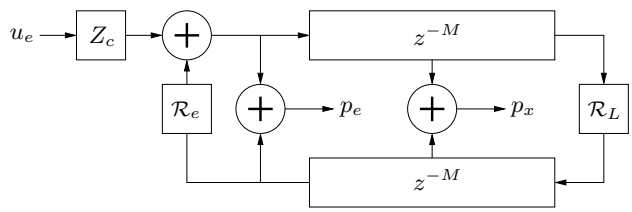

Figure 10: *A digital waveguide conical air column impedance model (from [4]).*

to discrete-time frequency "warping" and thus the results calculated with the DW model of Fig. 10 will be most accurate at frequencies well below half the sample rate.

If, as before, we are concerned only with the physical pressure at the input of the acoustic system modeled in Fig. 10, it is possible to commute the two delay lines to form the structure of Fig. 11.

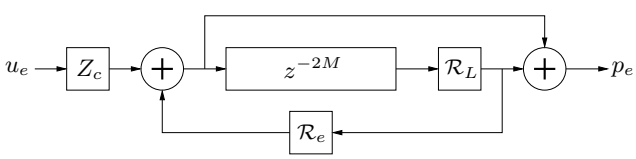

Figure 11: *The commuted digital waveguide input impedance model of a conical air column.*

The theoretical input impedance and impulse response of a conical section terminated with a load impedance as determined by [3] is shown in Fig. 12, calculated using both a frequency-domain [6] model and the DW structure of Fig. 11. Propagation losses along the length of the pipe were ignored in both cases.

The authors of [8] propose an alternate digital impedance model of a conical air column based again on an ideal open-end impedance approximation of $Z_L = 0$. Note that this approximation is less accurate with increasing open-end radius, which can be significant in musical instruments constructed from conical air columns. They "calibrate" their results by adding losses to the system such that the first two impedance magnitude peak values are matched to theoretical values. Their structure is a transfer function representation of the input impedance expression

$$Z_e(f) = \frac{\frac{x_e}{c}\mathcal{D}(f)}{1 + \frac{x_e}{c}\mathcal{D}(f)\mathcal{C}^{-1}(f)}, \tag{13}$$

where $\mathcal{D}(f) = jf$ is a differentiation operator and $\mathcal{C}(f)$ is the input impedance of a cylindrical pipe with an ideal open-end as-

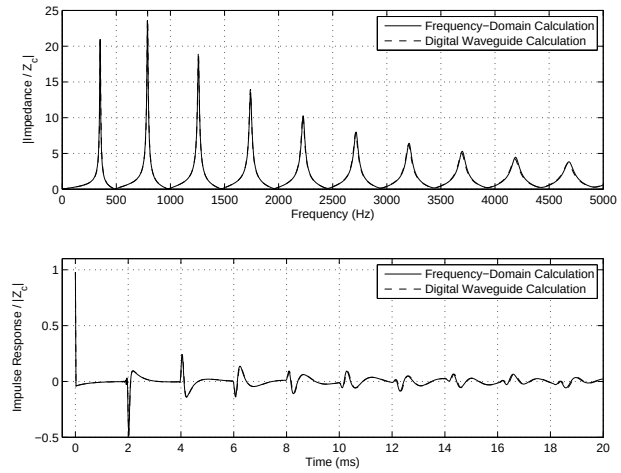

Figure 12: *Theoretical input impedance magnitude (top) and impulse response (bottom) of a conical section, relative to $|Z_c(e)|$ at the input end.*

sumption ($\mathcal{C}(f) = Z_0(f)$ as given by Eq. (7)). Figure 13 illustrates the computational structure used to implement this system, where $\mathcal{C}(f)$ is computed as in Fig. 6.

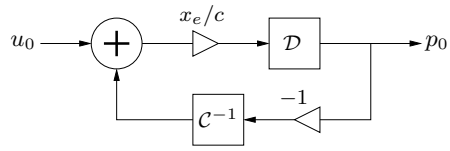

Figure 13: *Ideal impedance transfer function model of a conic section assuming $Z_L = 0$.*

The DW structures represented in Figs. 10 and 11 have a clear physical interpretation that supports the use of arbitrary filters to achieve as great a level of accuracy as needed for a given simulation. The structure of Fig. 13 is much more limited in this context.

4. THE REED INTERFACE

A pressure-controlled reed is traditionally modeled as a simple damped mechanical oscillator that is "displacement limited" by the mouthpiece facing. Assuming the reed motion is driven by the difference in pressures between the player's mouth and at the air column entrance, $p_\Delta = p_m - p_0$, this system can be expressed as

$$\frac{d^2y}{dt^2} + g_r \frac{dy}{dt} + \omega_r^2 y = -\frac{p_\Delta(t)}{\mu_r}, \tag{14}$$

where ω_r is the reed resonance frequency, g_r is the reed damping coefficient, and μ_r is the reed's dynamic mass per unit area. The flow through the reed channel is generally calculated using the Bernoulli equation and given by

$$u = w\,(y + H) \left(\frac{2\,|p_\Delta|}{\rho} \right)^{1/2} \mathrm{sgn}(p_\Delta), \tag{15}$$

where w is the reed channel width, y is the time-varying reed channel height, calculated from Eq. (14), and H is the equilibrium tip opening.

For single-reed geometries, the pressure and flow in the reed channel can be approximated as equivalent to the pressure and flow at the entrance to the instrument air column. This approximation is based on continuity and detachment of volume flow at the end of the reed channel such that pressure is not recovered in the mouthpiece. Thus, the acoustic interaction at the interface of the reed and air column can be solved using Eqs. (14) and (15), together with the DW input impedance computational structure of Fig. 3. From Fig. 3, it is clear that

$$p_0 = 2p_0^- + Z_c u_0, \tag{16}$$

where p_0^- is the traveling-wave pressure entering the reed junction from the downstream air column. This expression is also well known from [12]. Because of mutual dependencies, however, an explicit solution of these equations can be problematic. In a discrete-time computational context, these mutual dependencies can be understood to result in delay-free loops.

In [8], the reed system is discretized using a centered finite difference approximation that avoids a direct feedforward path through the reed transfer function. The resulting system equations can then be expressed in terms of a second-order polynomial equation and an explicit solution found.

The centered finite-difference approximation of Eq. (14) results in a digital filter structure of the form

$$\frac{Y(z)}{P_\Delta(z)} = \frac{-1/\mu_r}{(f_s^2 + \frac{g_r f_s}{2}) + (\omega_r^2 - 2f_s^2)z^{-1} + (f_s^2 - \frac{g_r f_s}{2})z^{-2}}, \tag{17}$$

where f_s is the computational sample rate. As noted in [13], however, this filter structure is only stable for $\omega_r < f_s\sqrt{4-(g_r/\omega_r)^2}$, limiting its use at low sample rates and/or with high reed resonance frequencies.

5. A STABLE REED FILTER

A direct application of the bilinear transform to the system of Eq. (14) results in a digital filter structure given by

$$\frac{Y(z)}{P_\Delta(z)} = \frac{-1/\mu_r\left[1+2z^{-1}+z^{-2}\right]}{a_0 + 2(\omega_r^2-\alpha^2)z^{-1} + (\alpha^2 - g_r\alpha + \omega_r^2)z^{-2}}, \tag{18}$$

where $a_0 = \alpha^2 + g_r\alpha + \omega_r^2$ and α is the bilinear transform constant that controls frequency warping. Note that we can achieve an exact continuous- to discrete-time frequency match at the resonance frequency of the reed by setting $\alpha = \omega_r/\tan(\omega_r/2f_s)$.

In this case, the use of the bilinear transform guarantees a stable digital filter at any sample rate. The presence of the direct feedforward path in Eq. (18), however, prohibits the explicit reed interface solution mentioned above. We therefore seek an alternative form of Eq. (18) that preserves stability and avoids an undelayed feedforward coefficient in the transfer function numerator.

By default, the bilinear transform substitution produces a system with "zeroes" at $z = \pm 1$ (or at frequencies of 0 and $f_s/2$ Hz). While this result is often desirable for digital resonators, we can modify the numerator terms without affecting the essential behavior and stability of the resonator. In fact, it is the numerator terms that control the phase offset of the decaying oscillation. Thus, we can modify and renormalize the numerator to produce a filter structure of the form

$$\frac{Y(z)}{P_\Delta(z)} = \frac{-4z^{-1}/\mu_r}{a_0 + 2(\omega_r^2-\alpha^2)z^{-1} + (\alpha^2 - g\alpha + \omega_r^2)z^{-2}}. \tag{19}$$

The frequency- and time-domain responses of the centered finite-difference and "modified" bilinear transform filter structures are shown in Fig. 14 for a reed resonance frequency $f_r = 2500$ Hz and $f_s = 22050$ Hz.

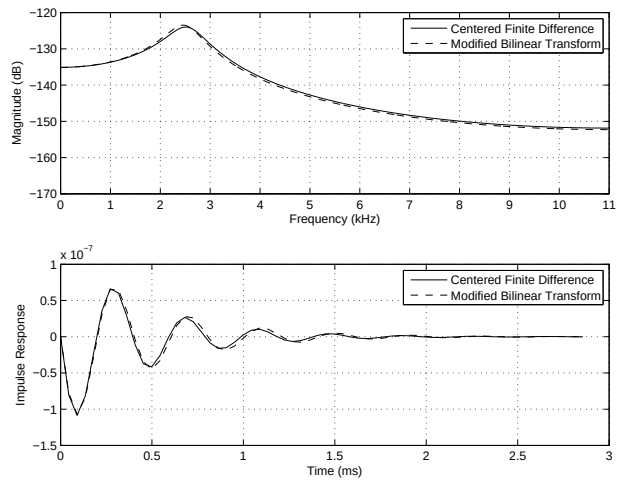

Figure 14: *Reed filter frequency and impulse responses for centered finite-difference and modified bilinear transform structures with $f_r = 2500$ Hz and $f_s = 22050$ Hz: magnitude frequency response (top) and impulse response (bottom).*

These plots are repeated in Fig. 15 for a reed resonance frequency $f_r = 8000$ Hz and $f_s = 22050$ Hz. It is clear that the centered finite-difference approximation is unstable in this case, while the modified bilinear transform solution remains accurate.

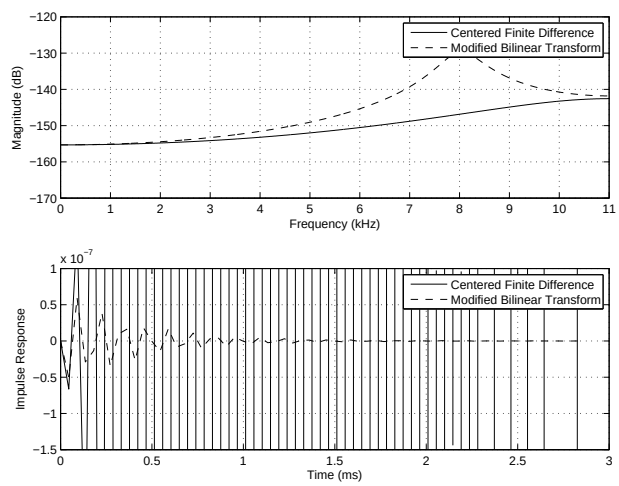

Figure 15: *Reed filter frequency and impulse responses for centered finite-difference and modified bilinear transform structures with $f_r = 8000$ Hz and $f_s = 22050$ Hz: magnitude frequency response (top) and impulse response (bottom).*

6. THE COMPLETE CLARINET MODEL

The complete clarinet model involves the calculation of the reed displacement using the stable reed model discussed in Section 5,

the volume flow through the reed channel as given by Eq. (15), and the relationship between flow and pressure at the entrance to the air column as given by Eq. (16). Because the reed displacement given by Eq. (19) does not have an immediate dependence on p_Δ, it is possible to explicitly solve Eqs. (16) and (15), as noted in [8], by an expression of the form

$$u_0 = 0.5\left(B\sqrt{(Z_c B)^2 + 4A} - Z_c B^2\right)\mathrm{sgn}(A), \qquad (20)$$

where $A = p_m - 2p_0^-$ and $B = w\,(y+H)(2/\rho)^{1/2}$ can be determined at the beginning of each iteration from constant and past known values. Whenever the reed position $y + H < 0$, u_0 is set to zero and $p_0 = 2p_0^-$.

In Fig. 16, the normalized pressure response of the complete DW synthesis model is plotted using both reed models with $f_r = 2500$ Hz and $f_s = 22050$ Hz. The behaviors are indistinguishable for these system parameters, though as indicated above it is possible to run the modified bilinear transform model at significantly lower sample rates (and with higher reed resonance frequencies).

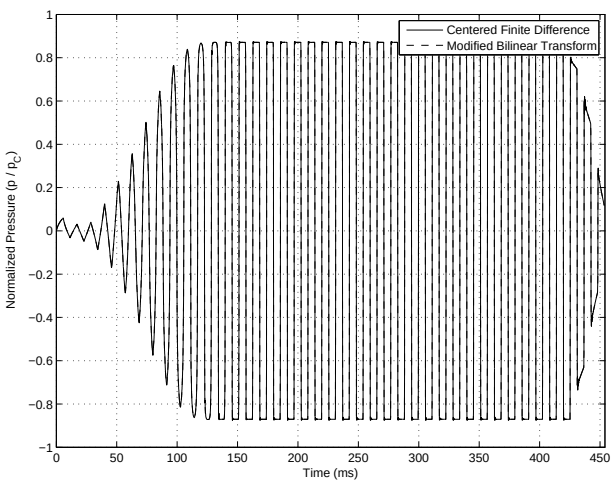

Figure 16: *Normalized pressure response from complete DW synthesis model using the centered finite-difference and modified bilinear transform structures with $f_r = 2500$ Hz and $f_s = 22050$ Hz.*

It should be noted that the explicit solution above is not possible if the reed is attached directly to a conical air column because the allpass truncation filter $\mathcal{R}_e$ of Fig. 10 creates a delay-free loop at the junction. Likewise, the differentiation operator in Fig. 13 presents the same limitation. A common solution to this problem, as discussed in [11], is to insert a short cylindrical section between the reed and conical waveguide of equivalent volume to the missing, truncated conic section.

7. CONCLUSIONS

We have presented a tutorial review on the use of digital waveguide techniques for the modeling of acoustic impedance in cylindrical and conical air column structures. The resulting systems are compared with digital impedance models recently discussed in the literature [8]. Both approaches simulate traveling-wave propagation using delay lines, though DW methods allow a more explicit and modular correlation between physical and computational components (for example, open-end filtering, toneholes, and radiation).

Further, we have presented a reed model that guarantees stability and an accurate continuous- to discrete-time resonance frequency mapping at any sample rate (assuming $f_r < f_s/2$). This model supports an explicit reed interface solution as proposed in [8].

8. REFERENCES

[1] J. O. Smith, "Efficient simulation of the reed-bore and bow-string mechanisms," in *Proc. Int. Comp. Music Conf. (ICMC'86),* Den Haag, Netherlands, 1986, pp. 275–280.

[2] ——, *Physical Audio Signal Processing: for Virtual Music Instruments and Digital Audio Effects*. W3K Publishing, 2004.

[3] H. Levine and J. Schwinger, "On the radiation of sound from an unflanged circular pipe," *Phys. Rev.*, vol. 73, no. 4, pp. 383–406, Feb. 1948.

[4] G. P. Scavone, "An acoustic analysis of single-reed woodwind instruments with an emphasis on design and performance issues and digital waveguide modeling techniques," Ph.D. dissertation, Music Dept., Stanford University, Mar. 1997.

[5] V. Välimäki, "Discrete-time modeling of acoustic tubes using fractional delay filters," Ph.D. dissertation, Helsinki University of Technology, Faculty of Electrical Engineering, Laboratory of Acoustic and Audio Signal Processing, Espoo, Finland, Report no. 37, Dec. 1995.

[6] D. H. Keefe, "Acoustical wave propagation in cylindrical ducts: Transmission line parameter approximations for isothermal and nonisothermal boundary conditions," *J. Acoust. Soc. Am.*, vol. 75, no. 1, pp. 58–62, Jan. 1984.

[7] C. A. Desoer and E. S. Kuh, *Basic Circuit Theory*. New York: McGraw-Hill, 1969.

[8] P. Guillemain, J. Kergomard, and T. Voinier, "Real-time synthesis of clarinet-like instruments using digital impedance models," *J. Acoust. Soc. Am.*, vol. 118, no. 1, pp. 483–494, July 2005.

[9] M. R. Schroeder, "Natural-sounding artificial reverberation," *J. Audio Eng. Soc.*, vol. 10, no. 3, pp. 219–223, 1962.

[10] A. H. Benade, "Equivalent circuits for conical waveguides," *J. Acoust. Soc. Am.*, vol. 83, no. 5, pp. 1764–1769, May 1988.

[11] G. P. Scavone, "Time-domain synthesis of conical bore instrument sounds," in *Proc. Int. Comp. Music Conf. (ICMC'02),* Gothenburg, Sweden, 2002, pp. 9–15.

[12] M. E. McIntyre, R. T. Schumacher, and J. Woodhouse, "On the oscillations of musical instruments," *J. Acoust. Soc. Am.*, vol. 74, no. 5, pp. 1325–1345, nov 1983.

[13] P. Guillemain, "A digital synthesis model of double-reed wind instruments," *EURASIP J. on Applied Sig. Proc.*, vol. 4, no. 7, pp. 990–1000, June 2004.